ASB/ISB award paper

Manipulating the edge of instability

Madhusudhan Venkadesan[a,*], John Guckenheimer[b], Francisco J. Valero-Cuevas[a]

[a]*Neuromuscular Biomechanics Laboratory, Sibley School of Mechanical & Aerospace Engineering, Cornell University, Ithaca, NY 14853, USA*
[b]*Department of Mathematics, Cornell University, Ithaca, NY 14853, USA*

Abstract

We investigate the integration of visual and tactile sensory input for dynamic manipulation. Our experimental data and computational modeling reveal that time-delays are as critical to task-optimal multisensory integration as sensorimotor noise. Our focus is a dynamic manipulation task "at the edge of instability." Mathematical bifurcation theory predicts that this system will exhibit well-classified low-dimensional dynamics in this regime. The task was using the thumbpad to compress a slender spring prone to buckling as far as possible, just shy of slipping. As expected from bifurcation theory, principal components analysis gives a projection of the data onto a low dimensional subspace that captures 91–97% of its variance. In this subspace, we formulate a low-order model for the brain + hand + spring dynamics based on known mechanical and neurophysiological properties of the system. By systematically occluding vision and anesthetically blocking thumbpad sensation in 12 consenting subjects, we found that vision contributed to dynamic manipulation only when thumbpad sensation was absent. The reduced ability of the model system to compress the spring with absent sensory channels closely resembled the experimental results. Moreover, we found that the model reproduced the contextual usefulness of vision only if we took account of time-delays. Our results shed light on critical features of dynamic manipulation distinct from those of static pinch, as well as the mechanism likely responsible for loss of manual dexterity and increased reliance on vision when age or neuromuscular disease increase noisiness and/or time-delays during sensorimotor integration.
© 2007 Published by Elsevier Ltd.

Keywords: Multisensory; Feedback; Motor control; Time-delay; Hand; Biomechanics

1. Introduction

Dynamic sensorimotor behaviors are quintessentially complex, nonlinear and high-dimensional, making it challenging to gain insight into their underlying neural control (Valero-Cuevas, 2005). For example, we handle objects easily without looking at them, but rely on vision when our fingers are numb. Revealing the mechanism behind this contextual use of vision is also of clinical value, since it can provide critical insight into why we drop objects more frequently as we grow old. Using a novel mechanics-based approach to experimentally and mathematically characterize dynamic manipulation we give an explanation for the contextual use of vision (Cole and Abbs, 1988; Johansson et al., 1992; Häger-Ross and Johansson, 1996; Cole et al., 1998; Augurelle et al., 2003) in the framework of task-optimal multisensory integration (Ernst and Bulthoff, 2004).

Most nonlinear dynamical systems exhibit low-dimensional dynamics at the edge of instability according to mathematical results from bifurcation theory (Guckenheimer and Holmes, 1983). The center manifold theorem states that the dynamics of high-dimensional systems at the edge of instability reduces to a low dimensional normal form on a center manifold (Guckenheimer and Holmes, 1983). Based on this insight, we designed an experiment where compressing a slender spring using the thumbpad (Fig. 1) brought the fused thumb + spring + nervous system to the edge of instability (Valero-Cuevas, 2000; Valero-Cuevas et al., 2003; Venkadesan et al., 2005). Motivated by spring buckling mechanics (Timoshenko, 1961; El Naschie, 1990), we hypothesized that the dominant dynamics of the fused thumb + spring + nervous system at the edge of instability will resemble a subcritical pitchfork bifurcation.

---

*Corresponding author. Tel.: +1 607 255 0990; fax: +1 607 255 1222.
E-mail address: mv72@cornell.edu (M. Venkadesan).
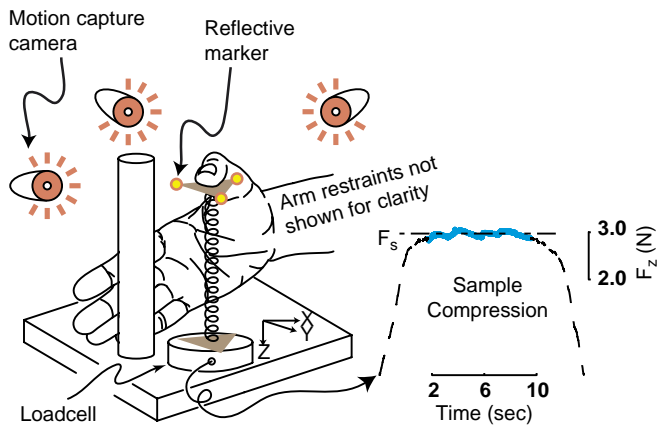*URL:* http://www.mae.cornell.edu/valero (M. Venkadesan).

Fig. 1. Schematic of the experimental setup. A representative sample compression is shown on the right, where a subject slowly compressed the spring to minimize the volume of the audio feedback provided (not shown), without letting the spring slip and maintained that compression for 7 s before slowly releasing the spring. For the sake of clarity, we have not shown the hand and arm restrains.

We use our data to test the additional hypothesis that task-optimal multisensory integration in the presence of both noise and time-delays explains the contextual use of vision depending on the availability/quality of digital sensors. The time-delays of interest in the context of multisensory integration are only those arising from sensory transduction, nerve conduction and neural processing. Previous studies on multisensory integration (Wolpert et al., 1995; van Beers et al., 2002; Ernst and Bulthoff, 2004; Körding and Wolpert, 2004; Kuo, 2005; Sober and Sabes, 2005) revealed that the relative utility of redundant sensory channels depends on their respective noisiness. For example, (Wolpert et al., 1995) applied Bayesian inference to study the effect of sensory noise but ignored effects of time-delays. However, both noise and time-delays are pervasive in the nervous system and affect sensorimotor control (Collins and Deluca, 1994; Cabrera and Milton, 2002). This suggests that the nervous system uses a task-optimal multisensory integration strategy that combines effects of noise and time-delays in each of vision, thumbpad sensation and non-digital sensors (e.g., muscle spindles, golgi tendon organ, and non-digital cutaneous afferents).

2. Methods

After giving written informed consent, nine males and three females (19–40 years of age, mean = 23 years) participated in our study that was approved by the Cornell University Committee on Human Subjects. All subjects were right-handed, healthy young adults with no known impairments or recent injuries to their hand and had normal visual acuity or normal with correction. They had no prior experience with this experimental task.

2.1. Experimental setup

Subjects were asked to compress a slender helical spring prone to buckling using just their thumbpad (Venkadesan et al., 2005) (Fig. 1). The design specifications for the spring are—free length = 76.2 mm, mean diameter = 8.7 mm, wire diameter = 0.79 mm, total coils = 24, material:

music wire (#12201, Century Spring Corp., Los Angeles, CA), which we mounted in polymer (ABS P400) endcaps. The top endcap was flat (friction coefficient ~0.5) with a small (0.1 mm) conical projection, precisely coincident with the cylindrical axis of the spring, providing a tactile cue for its geometric center. We mounted the spring on a uniaxial load cell (SML-25, Interface Inc., Scottsdale, AZ), and logged vertical compressive force at 1000 Hz using a 16-bit analog-to-digital data acquisition system. We also recorded 3D location and orientation of the spring's endcap at 200 Hz using a 4-camera motion capture system (Vicon Peak, Lake Forest, CA; Fig. 1) that tracked the three reflective markers attached to the top endcap. We did not use any digital filters on either the force or the motion data for our analyses.

The thumb rested on the endcap with the distal phalanx horizontally oriented, fingers curled around a vertical post and the forearm fixed using a vacuum pillow (Versa Form, Sammons Preston Roylan, Bolingbrook, IL) with the wrist placed in neutral flexion–extension/ad-abduction (Fig. 1) and the elbow at 90° flexion. We did not fix the base of the thumb or the wrist since non-digital mechanoreceptors could contribute to object manipulation (Häger-Ross and Johansson, 1996). Subjects could view the entire spring–thumb assembly from a self-selected angle and their palm never touched the spring.

We provided audio feedback using a clearly audible 500 Hz tone that linearly decreased in volume as the vertical compressive spring force increased. We calibrated this inverse relationship so that no subject made the tone faint enough to be inaudible since the volume vanished only when the compressive force exceeded 4 N, which was not attained by any subject.

2.2. Experimental protocol

We instructed subjects to, "Slowly compress the spring using only your thumbpad to make the tone volume as faint as possible (i.e., maximize vertical compressive spring force) without letting the spring slip. Once you have reached the point where you cannot decrease the tone volume without letting the spring slip, hold the compressive load so that the tone volume, although now faint, remains constant and slowly release the spring after 10 s. It does not matter if the spring bends or oscillates, it only matters that the volume stays constant once you reach the minimum attainable volume and that the spring does not slip." Only trials with loading/unloading rate less than 5 N/s were considered "successful".

2.3. Metric of performance: F_s

The mean compressive spring force during the sustained hold phase was the metric of performance (F_s). The hold phase was "sustained" if the coefficient of variation (COV) of the compressive spring force was less than 5% for 7 s. We used three largest F_s values of ten attempts per treatment condition per subject as repeated measures for our statistical analyses. We provided over 1 min rest after every five compressions.

2.4. Experiments to test for effects of training, loss of vision and thumbpad sensation

The experiment was performed over 2 days. On day 1, subjects performed 100 compressions of training and we measured their performance before and after training with normal visual and thumbpad sensibility. On day 2, we first measured performance with normal thumbpad sensibility, both with and without vision. An experienced hand surgeon then administered 5 cc of 1% Lidocaine solution on the ulnar and radial sides of the base of the thumb (just below the metacarpophalangeal (MCP) joint of the thumb, but away from the thenar eminence) to obtain a digital nerve-block without affecting any musculature (and associated sensors). Cutaneous sensation proximal to the thumb MCP joint was unaffected (tested using the same procedure used below). The nerve-block was considered effective when vision-occluded subjects could not detect a 10 g load randomly moved across or applied on their thumbpad using a

pointed tip. The point-load was applied using a pair of forceps (weighing 10 g) that was lightly held at its base by the experimenter while the pointed end rested on the subject's skin surface to be tested for sensitivity. Note that subjects could detect the small pointed projection at the center of the spring's endcap by pressing their thumbpad forcefully. We then measured task performance after the loss of digital cutaneous sensation, both with and without vision.

We measured maximum isometric force that subjects could produce in two postures, namely key and opposition pinch postures (Valero-Cuevas et al., 2003) using a pinch meter before the nerve block on both days. The largest reading of three attempts was recorded as pinch strength. We gave over 2 min rest at the end of strength measurement and extra rest if asked for.

2.5. Safety-margin of F_s

To see if subjects reached a compressive force consistently shy of the force at spring slip (safety-margin), we tested whether F_s or F_{max} (maximum compressive load) changed for successful vs. slipped trials. We redefined F_s when the spring slipped by requiring only a 3 s hold for being a "successful" trial, since slippage often occurred before 7 s elapsed.

2.6. Analysis of endcap rotation

To analyze 3D endcap rotation we calculated the unit normal vector to the plane of the endcap and determined whether one principal component could explain most of the endcap rotation. We then tested whether the rotation projected onto its first principal component (θ_{range}) varied with F_s as predicted by the subcritical pitchfork bifurcation normal form (Eq. (1)) using a nonlinear least square regression. The central region around the solid line at $\theta = 0$ bounded by the dashed curves in Fig. 2 is the domain of attraction, which narrows with increasing F_s, i.e., it is the predicted θ_{range} as the spring is compressed when the spring does not slip. We also performed a linear regression of endcap rotation projected onto the second principal component vs. F_s.

We chose endcap angle as the kinematic variable for our analyses because of the typical spring profile observed during experiments (Fig. 2, left). The spring was typically laterally displaced from the centerline (allowed by task instructions—"It does not matter if the spring bends…"), but the endcap remained nearly horizontal for successful trials and rapidly rotated away from horizontal for slipped trials. This suggested that endcap angle best captured the relevant dynamics of active control.

2.7. Statistical analyses

The independent treatments were training and available sensory modalities. The dependent variable for all our statistical analyses was F_s, except for the "safety-margin" analyses, where F_{max} was an additional dependent variable. We had six treatments: (i) Day 1, pre-training, (ii) Day 1, post-training, and (iii)–(vi) Day 2, four combinations of presence/absence of vision/thumbpad sensation. We set $\alpha = 0.025$ as the threshold for significance, since we performed two repeated-measures ANOVAs: (i) effect of the above six treatments with planned comparisons as post hoc tests, and (ii) effect of slip vs. no-slip for all six treatments. Subjects were random factors for all ANOVAs.

We also performed a multiple regression analysis of F_s vs. key and opposition pinch strength using an ANCOVA. Subjects were random factors and the six treatments were fixed factors. Since a mixed factor ANCOVA does not provide a model R^2, we used a regular ANCOVA to determine approximate model R^2.

We verified necessary assumptions for the validity of each ANOVA/ANCOVA, namely, normality and identical distribution of the residuals. We used SAS (SAS, Cary, NC) for all statistical analyses.

2.8. Mathematical modeling of multisensory integration

We modeled the overall 1D dynamics of the closed-loop system as a subcritical pitchfork bifurcation of the endcap angle (θ) projected onto its
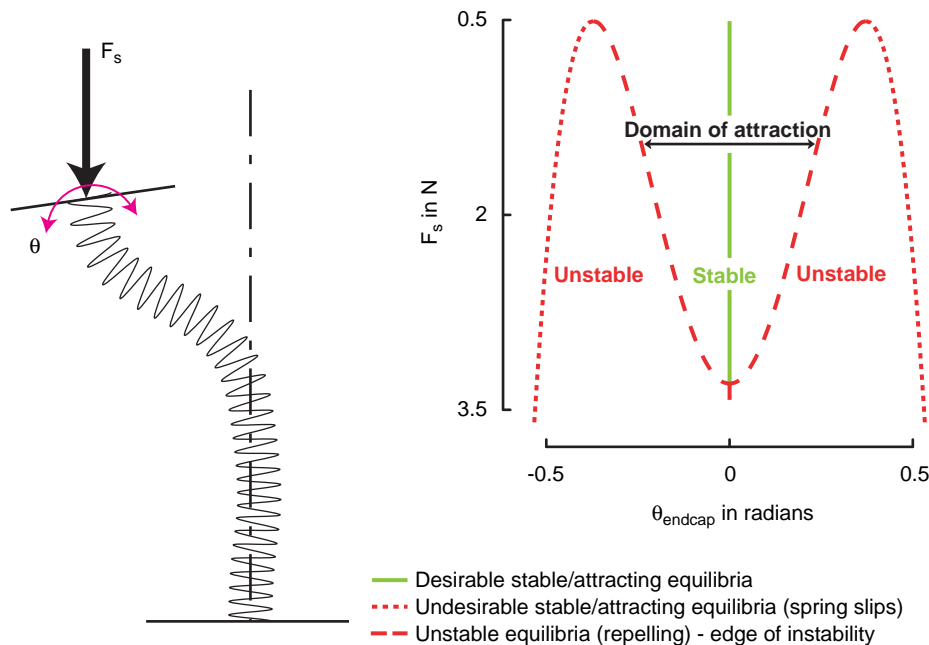

Fig. 2. Subcritical pitchfork bifurcation diagram. The bifurcation diagram on the right shows the loci of both stable (solid line) and unstable/undesirable (dashed/dotted curves) equilibria for the thumb + spring + nervous system's closed loop dynamics without noise or time-delays as the spring is compressed, which is a succinct description of the underlying deterministic (no time-delays/noise) dynamics of our model. The region bounded by the dashed curves around $\theta = 0$ (the endcap orientation we want to stabilize), in which the endcap is attracted towards $\theta = 0$ is the domain of attraction at any particular value of F_s. If the endcap strays too far outside this region, then it will be rapidly attracted towards the points far out (dotted curves, close to 0.5 rad), which is representative of a spring slip. The schematic of a buckled spring on the left clarifies the physical meaning of the variables F_s and θ.

first principal component, given by (Fig. 2)

$$\dot{\theta} = \alpha(F_s - K)\theta + \beta\theta^3 - \gamma\theta^5, \qquad (1)$$

where, α, β and γ are scaling parameters, F_s represents compressive spring force and K represents the maximum attainable compressive spring force or equivalently, effective feedback gain.

We incorporated multisensory feedback using a simple proportional controller with input a weighted sum of three sensory signals (Fig. 3, Eq. (2)): thumbpad sensation, non-digital mechanoreceptors, and vision. We added zero-mean Gaussian white noise ($N_i(0, \sigma_i^2)$; $i = 1, 2, 3$) and a constant time-delay (τ_1, τ_2, τ_3) to each sensory signal and assumed that all sensors were unbiased (mean(θ_i^{sen}) = θ).

Human visual acuity is known to be at least 1 min arc at a viewing distance of 250 mm (Liang and Westheimer, 1993; Saunders and Knill, 2004). Subjects' heads were typically 100–170 mm from the spring in our experiment. Because the endcap radius was 40 mm, the estimated standard deviation for visual sensation was $\sigma_3 = 0.0009$ rad. Estimated standard deviation of thumbpad sensation based on reported tactile discrimination ability (Wheat et al., 1995) was $\sigma_1 = 0.0007$ rad. To account for the reported unreliability of non-digital mechanoreceptors (Häger-Ross and Johansson, 1996; Macefield and Johansson, 1996), we used $\sigma_2 = 0.003$ rad ($10 \times$ the variance of vision). Since the greatest F_s load that subjects could stabilize was ≈ 3 N, we chose the proportional feedback constant $K = 3.3$ (90% of $3.3 \approx 3$). The spring slips only when the angle of the endcap with respect to the horizontal exceeds the friction angle (~ 0.5 rad). We could directly solve α/γ and β/γ so that the mean friction angle (dotted curve in Fig. 2) was 0.5 and was never less than 0.4 (80% of the average) since there are two unknowns (α/γ, β/γ) and two equations (mean and minimum of friction angle).

We tuned γ (time-scale, the only parameter we could not determine from frictional or neurophysiological properties) so that for physiologically realistic time-delays and noise, the simulation (with time-delays and noise) yielded F_s values within experimental range when both thumbpad sensation and vision were occluded. The resulting model is given by the following equations (Fig. 3):

$$\frac{d\theta}{dt} = \overbrace{\alpha F_s \theta(t) + \beta\theta(t)^3 - \gamma\theta(t)^5}^{\text{Subcritical pitchfork bifurcation normal form equation}}$$

$$- \overbrace{\alpha K \hat{\theta}(t, t - \tau_1, t - \tau_2, t - \tau_3)}^{\text{Proportional feedback using estimated task-relevant parameter}}$$

$$\hat{\theta} = \sum_{i=1}^{3} \omega_i(\theta(t - \tau_i) + \sigma_i v_i); \quad \text{task-relevant parameter estimate}$$

$$v_i \sim \underbrace{N_i(0, 1); \quad i = 1, 2, 3;}_{\text{independent Gaussian white noise processes}} \qquad (2)$$

where, $\alpha = 2.639$, $\beta = 106.512$, $\gamma = 385$, $K = 3.3$ and the time-delays are, $\tau_1 = 65$ ms (Cole and Abbs, 1988; Johansson et al., 1992; Eliasson et al., 1995; Kandel et al., 2000; Johansson and Birznieks, 2004), $\tau_2 = 65$–120 ms in 5 ms increments to model the large variability in reported time-delay for non-digital sensors (Cole and Abbs, 1988; Johansson et al., 1992; Eliasson et al., 1995; Kandel et al., 2000; Johansson and Birznieks, 2004), $\tau_3 = 120$ ms (Prablanc and Martin, 1992; Paillard, 1996; van Beers et al., 2002).

2.9. Numerical optimization

The objective function, namely, performance, was F_s, numerically defined so that the endcap is stable ($\theta < 0.5$ rad) for 80% ($\pm 5\%$) of the trials ("success-rate") during the 7 s hold ("survival-time"). Using success-rates and survival-times to define the metric of performance is necessary for stochastic differential equations such as Eq. (2) (Cabrera and Milton, 2004). We performed an exhaustive search of all possible sensory weights (2D optimization problem; supplementary notes) to find task-optimal sensory weights. Additionally, we compared task-optimal sensory weights against weights that minimize the effect of noise alone (as hypothesized by Bayesian inference for static tasks) (Ernst and Bulthoff, 2004) using the formula $\omega_i = (1/\sigma_i^2)/\sum_j(1/\sigma_j^2)$, where ω are sensory weights and σ^2 are the variances of each sensory modality. All simulations used the MATLAB® environment.

3. Results

Principal components analysis revealed that the experimentally measured endcap rotation collapsed to 1D at the edge of instability, and the stable domain of attraction shrunk with increasing compressive spring force in close resemblance to the subcritical pitchfork bifurcation normal form equation (Fig. 4a and b). The first principal component explained 94.5% of the variance in 3D motion of the unit normal vector (99.9% confidence interval = (91.2%, 96.6%)), i.e., rotation about one fixed axis described almost 95% of endcap rotational dynamics. The experimentally obtained relationship between range of endcap rotation along the first principal axis vs. F_s (Fig. 5a: solid curve, $\hat{\alpha}_{estimate} = 0.0017$, $\hat{\beta}_{estimate} = 0.11$, $K_{estimate} = 3.45$, $R^2 = 0.32$) agreed well with the mechanics-based (namely, frictional constraints) model
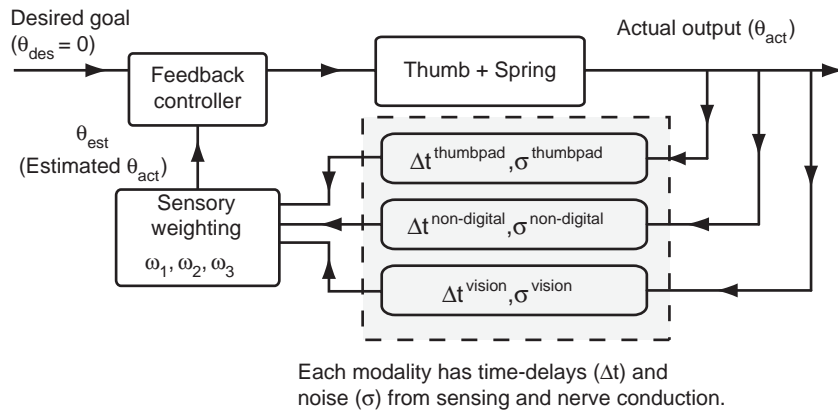

Fig. 3. A block diagram showing feedback control using three sensory modalities, namely: (1) thumbpad sensation, (2) non-digital mechanoreceptors, and (3) vision. The mathematical model is a specific implementation of this block diagram that uses simple proportional feedback control and the entire closed-loop dynamics of this system is modeled as a subcritical pitchfork bifurcation. Time-delays (Δt) and noise (σ) are explicitly labeled only for the sensory branches since for the purpose of this study, only the sensory time-delays and noise affect the relative usefulness of various modalities.
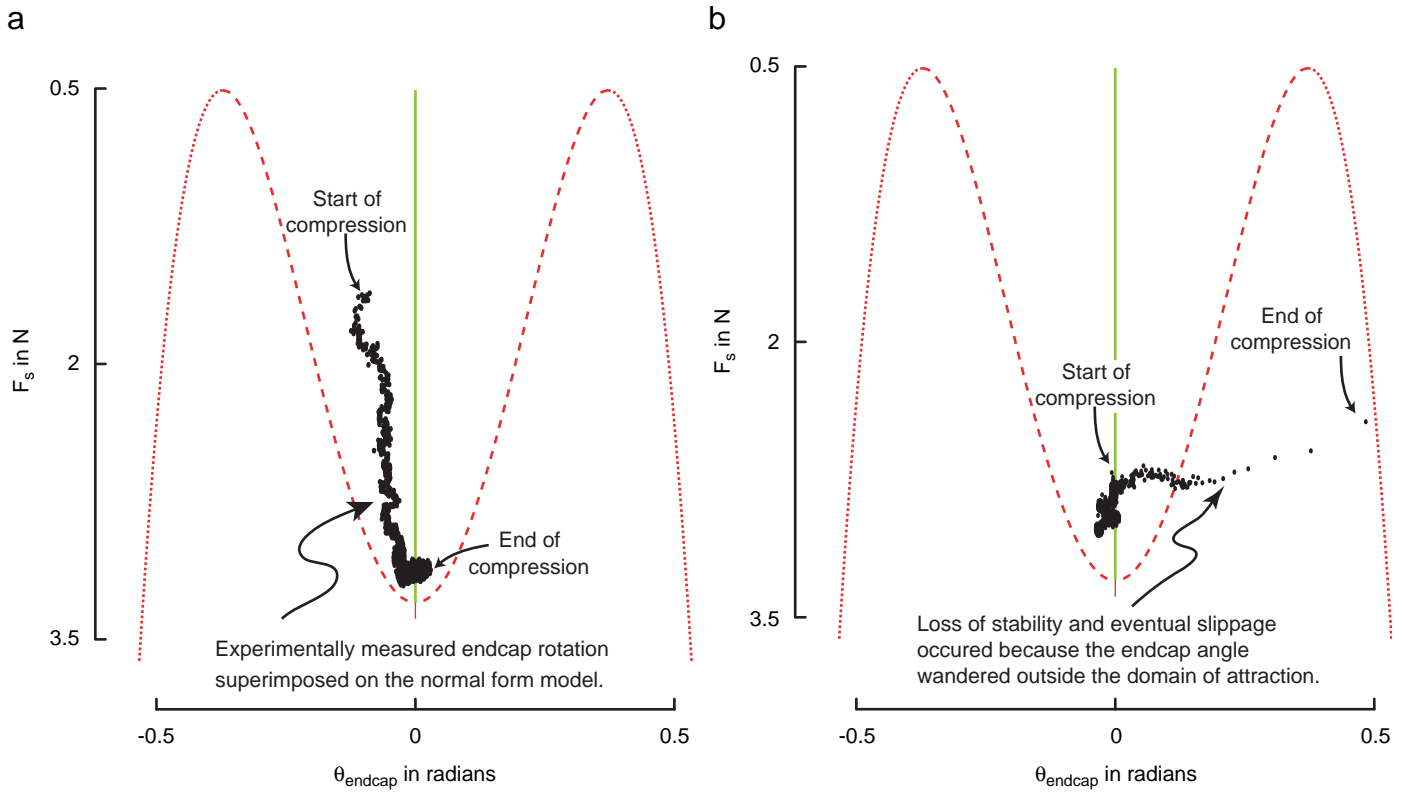
a

b

Fig. 4. (a) Representative trial showing endcap rotation time-history for a successful trial. This trial was with all sensations intact. Note how the endcap rotation is better regulated as the compressive spring force increases. Importantly, the endcap rotation angle stays well within the domain of attraction predicted by the subcritical pitchfork bifurcation normal form. (b) Representative trial showing endcap rotation time-history when the spring slipped. This trial was with all sensations intact. Note that the spring slipped when the endcap rotation angle exceeded the domain of attraction. Importantly, the load at slip was lower than when the spring did not slip (cf. Fig. 4a).
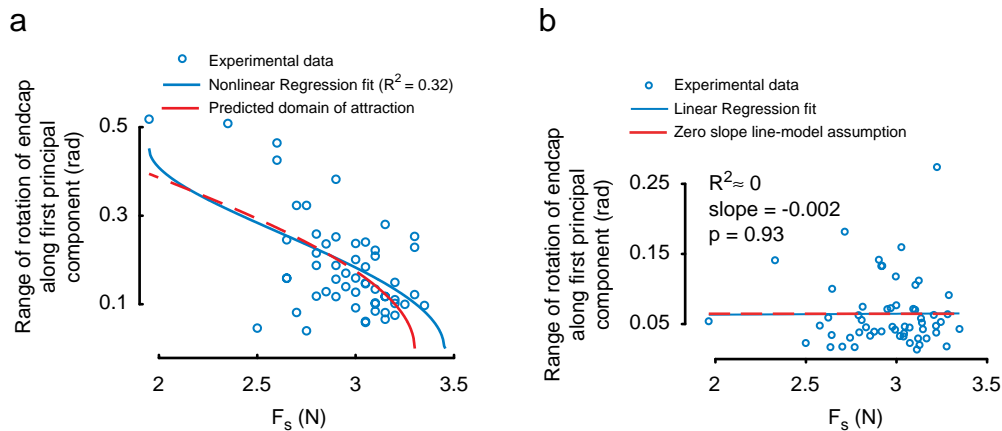
a

b

Fig. 5. (a) The first principal component captures all relevant endcap rotational dynamics. The spatiotemporal dynamics of the normal form model were indistinguishable from experimental measurements projected onto the first principal component. The best nonlinear least squares fit for the relationship between range of endcap rotation vs. F_s along the first principal components is nearly identical to model prediction for a subcritical pitchfork bifurcation (Fig. 3). The low R^2 means that the system is very noisy. (b) The independence of the dynamics (range of endcap rotation) from F_s (slope indistinguishable from 0) along the second principal component further supports our model rationale since it indicates that all relevant endcap rotational dynamics were captured by the first principal component and the second component provides no additional information.

prediction (Eq. (1), Fig. 5a: dashed curve, $\hat{\alpha}_{model} = 0.0069$, $\hat{\beta}_{model} = 0.28$, $K_{model} = 3.3$). Further, the range of endcap rotation along the second principal component showed no dependence on F_s (Fig. 5b; slope = 0, $p = 0.96$, $R^2 \approx 0$).

Experimentally, the occlusion of vision had a measurable impact on performance only when thumbpad sensation was also occluded (Fig. 6a). When thumbpad sensation was lost, F_s always decreased (With vision : F_s^{normal} −
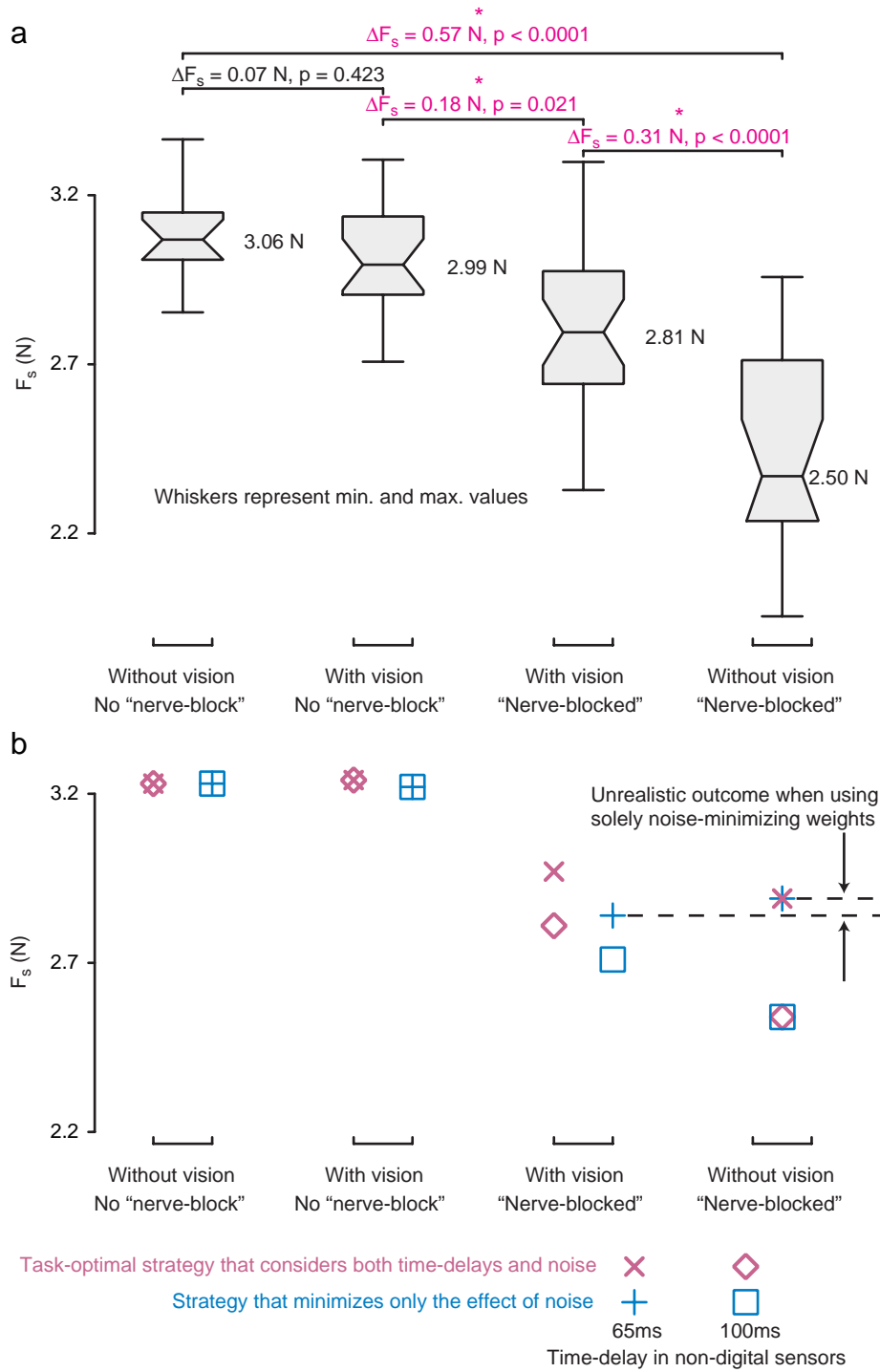
Fig. 6. (a) Box plots of experimental results of sensory occlusion. The horizontal bars inside the box plots is the median, the notches are the robust 95% confidence interval of the median, the boxes are bounded by the 75th percentile and 25th percentile, the numeric values next to each box is the sample mean, and the whiskers represent the entire range of the data. The expected contextual use of vision is found by comparing columns 1 vs. 2 and columns 3 vs. 4. The differences in F_s marked with a '∗' symbol are the only significant ones at the preset significance level of 0.025. (b) Results of simulations using two alternate sensory weighting strategies. Only simulations with 65 ms time-delay for non-digital sensors ('×', '+') and with 100 ms time-delay for non-digital sensors that best replicated experimental data ('◇', '□') are shown above. The task-optimal strategy ('×', '◇') yields better performance (larger F_s) than the noise-minimizing strategy ('+', '□') demonstrating the effect of time-delays on multisensory integration. The 100 ms-*simulation* ('◇', '□') using a task-optimal strategy ('×', '◇') best agreed with experimental data (cf. 3rd vs. 4th columns). Noise-minimizing sensory weights ('+', '□'), however, yield unrealistic and non-robust results such as an increase in performance after visual occlusion over and above loss of thumbpad sensation (again, cf. 3rd vs. 4th columns). Note that when both thumbpad sensation and vision are absent there is no multisensory integration required since only the non-digital mechanoreceptors remain intact. The sensory weights used in the simulations are listed in Table 1.

Table 1
Task-optimal and noise-minimizing sensory weights for all simulations

Sensory conditions	No vision no "nerve-block"		With vision no "nerve-block"		With vision "nerve-blocked"		No vision "nerve-blocked"
Strategy[a]	TO	NM	TO	NM	TO	NM	TO = NM
Simulations with $\tau_{\text{non–digital}} = 65\,\text{ms}$							
Digital (ω_1)	0.96	0.95	0.96	0.65	–	–	–
Non-digital (ω_2)	0.04	0.05	0.04	0.03	0.35	0.09	1
Visual (ω_3)	–	–	0	0.32	0.65	0.91	–
Simulations with $\tau_{\text{non–digital}} = 100\,\text{ms}$							
Digital (ω_1)	0.99	0.95	0.95	0.65	–	–	–
Non-digital (ω_2)	0.01	0.05	0	0.03	0.27	0.09	1
Visual (ω_3)	–	–	0.05	0.32	0.73	0.91	–

The columns of sensory weights in this table correspond to the columns in Fig. 6b.
[a] TO: task-optimal; NM: noise-minimizing.

Table 2
Statistical post hoc planned comparisons of F_s (sustained load) and $F_{\max}$ (maximal load) for trials when the spring slipped vs. when the spring did not slip

Subject condition	$\Delta F_s = F_s^{\text{slip}} - F_s^{\text{no-slip}}$ (N)	*p*-value	$\Delta F_{\max} = F_{\max}^{\text{slip}} - F_{\max}^{\text{no-slip}}$ (N)	*p*-value
Normal	0.01	0.912	0.03	0.708
No vision	0.15	0.530	−0.07	0.688
Nerve-blocked	0.05	0.667	0.12	0.197
No vision, nerve-blocked	−0.01	0.900	0.03	0.700

The above values are all for Day 2. These results indicate that subjects did not maintain a "safety margin" during the successful (i.e., no-slip) performance of this dynamic manipulation task. The ANOVA across conditions, was significant with $p < 0.0001$.

$F_s^{\text{numb}} = 0.18\,\text{N}$, $p = 0.021$; Without vision : $F_s^{\text{normal}} - F_s^{\text{numb}} = 0.57\,\text{N}$, $p < 0.0001$; Fig. 6a). After visual occlusion however, F_s remained unchanged when the thumbpad was intact (Intact thumbpad : $F_s^{\text{vision}} - F_s^{\text{blind}} = -0.07\,\text{N}$, $p = 0.423$), but decreased by a large amount when the thumbpad was numb (Numb thumbpad : $F_s^{\text{vision}} - F_s^{\text{blind}} = 0.31\,\text{N}$, $p < 0.0001$).

Computationally (Eq. (2), Fig. 3), by using numerical optimization, we found that this contextual use of vision emerged for sensory weights (for thumbpad sensors, non-digital sensors and vision) that maximized performance (F_s), i.e., by accounting for both sensory noise and time-delays (Fig. 6b, Table 1) despite large uncertainty in time-delay for non-digital sensors (closest match to experimental data when $\tau_{\text{non–digital}} = 100\,\text{ms}$). In contrast, purely noise-minimizing sensory weights (disregarding time-delays) led to unrealistic results such as an improvement in performance after loss of vision and thumbpad sensation (Fig. 6b column 3 vs. 4 when $\tau_{\text{non–digital}} = 65\,\text{ms}$).

Training had no effect on F_s on day 1 (Day 1 : $F_s^{\text{post-train}} - F_s^{\text{pre-train}} = 0.08\,\text{N}$, $p = 0.248$). Performance on day 2 was also not statistically different from that on day 1 (numerically greater by 0.05 N and lower by 0.03 N than the start and end of day 1, respectively).

Subjects did not maintain any consistent "safety-margin", indicating that they were truly at their sensor-imotor limit when sustaining maximal compression of the spring. There was no difference in F_s or $F_{\max}$ between successful trials vs. when the spring slipped for all four sensory occlusion conditions ($p > 0.530$, $p > 0.197$, respectively; Table 2).

The COV of pinch strength (mean = 99.41 N, COV = 13.8%) was almost three times that of F_s with normal sensibility on day 2 (mean = 2.99 N, COV = 5.2%, < 5% of pinch strength). Moreover, a multiple regression of F_s for all sensory conditions on day 2 vs. static pinch strength (key and opposition; $p = 0.969$, and 0.338, respectively, overall $R^2 = 0.66$) was statistically non-significant. The high R^2 indicates that one can reliably conclude that F_s was independent from strength.

4. Discussion

A mechanics-based low-order normal form equation from bifurcation theory produced dynamics indistinguishable from experimental measurements at the edge of instability in a dynamic manipulation task. Using this normal form equation, we successfully developed a model of multisensory integration which replicated the contextual use of vision found in our sensory occlusion experiments. The contextual use of vision was robust to neurophysiologically tenable uncertainty in the time-delay for non-digital sensors only for a task-optimal multisensory weighting strategy that accounted for both time-delays and noise. However, a static Bayesian inference strategy that accounted solely for noise did not possess this

robustness. Thus, we revealed the effect of time-delays over and above the known effects of noise on multisensory integration. It is worth noting the ability of our nonlinear low-order model to capture both the effects of sensory occlusion *and* the spatiotemporal dynamics of the task. Importantly, our model had only one free parameter (timescale for overall dynamics) and all other parameters were obtained from basic frictional constraints and previously reported neurophysiological data for sensory time-delays and noise variances.

Our study critically extends our understanding of the neural control of manipulation by indicating important differences between static and dynamic grasp. First, subjects did not maintain a detectable safety-margin when compressing the spring, unlike static grasp (Cole and Abbs, 1988; Johansson et al., 1992; Eliasson et al., 1995; Cole et al., 1998; Augurelle et al., 2003). Second, we found no relationship between dynamical performance (F_s) and pinch strength. The fact that our experimental paradigm focuses on very low forces ($F_s < 5\%$ of pinch strength) allows us to conclude that we are investigating the limit of hand sensorimotor integration, independently of muscle strength.

There are some limitations of this study that, while not affecting the validity of our results, do open new directions for future research. We argue that feedback control is used for preventing slippage at the edge of instability in contrast to a predictive forward/inverse dynamic model (Wolpert et al., 1995; van der Kooij et al., 1999; Kuo, 2005) or a preset thumbtip impedance (Burdet et al., 2001). When the spring + thumb + nervous system is close to the edge of instability, sensitivity to noise and other uncertainties increases dramatically (Stein, 2003), thus rendering unlikely, the use of time-delay compensation or predictive control. Also, sensory occlusion severely affected performance indicating that a preset (feedforward) thumbtip impedance was not the dominant form of control. This claim is further supported by preliminary evidence from a separate study (Valero-Cuevas et al., 2006). Moreover, a high-impedance strategy would be dependent on thumb strength (Hogan, 1984), and would be destabilizing due to signal-dependent noise in muscles (Harris and Wolpert, 1998). As with any modeling work, we cannot conclusively prove that the nervous system indeed uses a task-optimal strategy. Nevertheless, our results agree with and add valuable insight to the existing body of evidence for optimality principles in sensorimotor control (Harris and Wolpert, 1998; Todorov, 2004).

Our results are compatible with other studies of multisensory integration (Wolpert et al., 1995; Ernst and Bulthoff, 2004; Körding and Wolpert, 2004) and precision pinch (Cole and Abbs, 1988; Johansson et al., 1992; Augurelle et al., 2003), but go beyond them to investigate for the first time, multisensory integration during a complex, nonlinear and dynamic manipulation task. Our novel task—by virtue of being dynamic, unstable and nonlinear, and exploiting the dimensional collapse at the edge of instability—was able to reveal how both time-delays and noise affect multisensory integration, unlike past studies that used static task goals.

In summary, using mathematically predicted properties of nonlinear dynamical systems we find that dynamic manipulation at the edge of instability becomes mathematically tractable without compromising the complexity of the task or oversimplifying the analysis. We found that time-delays affect multisensory integration in addition to the previously known effects of noise and the contextual use of vision arises naturally from task-optimal multisensory integration. This work sheds light on the loss of dexterity with aging—by providing a paradigm within which to assess the different consequences of degradation of tactile sensors vs. increased cortical processing (i.e., "computational") time-delays (Cole et al., 1998) to the efficacy of multisensory integration for dynamic manipulation. Additionally, we found that the neural control of dynamic manipulation detects and regulates incipient instabilities such as an imminent slip. In conclusion, since the dimensional collapse at the edge of instability is ubiquitous in almost all nonlinear dynamical systems, we can extend this paradigm to other sensorimotor systems. Together with our simple, low-order mathematical model based on bifurcation theory, our novel and simple paradigm of pushing the combined body + world + nervous system to an edge of instability is a powerful tool that opens up research directions to reveal the nature of sensorimotor control in development, ageing, disease and treatment.

Appendix A. Supplementary material

Supplementary data associated with this article can be found in the online revision at doi:10.1016/jbiomech.2007.01.022.

References

Augurelle, A.S., Smith, A.M., Lejeune, T., Thonnard, J.L., 2003. Importance of cutaneous feedback in maintaining a secure grip during

manipulation of hand-held objects. Journal of Neurophysiology 89 (2), 665–671.

Burdet, E., Osu, R., Franklin, D.W., Milner, T.E., Kawato, M., 2001. The central nervous system stabilizes unstable dynamics by learning optimal impedance. Nature 414 (6862), 446–449.

Cabrera, J.L., Milton, J., 2004. Stick balancing: on-off intermittency and survival times. Nonlinear Studies 11 (3), 305–317.

Cabrera, J.L., Milton, J.G., 2002. On–off intermittency in a human balancing task. Physical Review Letters 89 (15).

Cole, K.J., Abbs, J.H., 1988. Grip force adjustments evoked by load force perturbations of a grasped object. Journal of Neurophysiology 60 (4), 1513–1522.

Cole, K.J., Rotella, D.L., Harper, J.G., 1998. Tactile impairments cannot explain the effect of age on a grasp and lift task. Experimental Brain Research 121 (3), 263–269.

Collins, J.J., Deluca, C.J., 1994. Random walking during quiet standing. Physical Review Letters 73 (5), 764–767.

El Naschie, M.S., 1990. Stress, Stability and Chaos in Structural Engineering: An Energy Approach. McGraw-Hill, London, New York.

Eliasson, A.C., Forssberg, H., Ikuta, K., Apel, I., Westling, G., Johansson, R., 1995. Development of human precision grip, 5. Anticipatory and triggered grip actions during sudden loading. Experimental Brain Research 106 (3), 425–433.

Ernst, M.O., Bulthoff, H.H., 2004. Merging the senses into a robust percept. Trends in Cognitive Sciences 8 (4), 162–169.

Guckenheimer, J., Holmes, P., 1983. Nonlinear Oscillations, Dynamical Systems, and Bifurcations of Vector Fields. Springer, New York.

Häger-Ross, C., Johansson, R.S., 1996. Nondigital afferent input in reactive control of fingertip forces during precision grip. Experimental Brain Research 110 (1), 131–141.

Harris, C.M., Wolpert, D.M., 1998. Signal-dependent noise determines motor planning. Nature 394 (6695), 780–784.

Hogan, N., 1984. Adaptive-control of mechanical impedance by coactivation of antagonist muscles. IEEE Transactions on Automatic Control 29 (8), 681–690.

Johansson, R.S., Birznieks, I., 2004. First spikes in ensembles of human tactile afferents code complex spatial fingertip events. Nature Neuroscience 7 (2), 170–177.

Johansson, R.S., Häger-Ross, C., Backstrom, L., 1992. Somatosensory control of precision grip during unpredictable pulling loads, 3. Impairments during digital anesthesia. Experimental Brain Research 89 (1), 204–213.

Kandel, E.R., Schwartz, J.H., Jessell, T.M., 2000. Principles of Neural Science. McGraw-Hill, Health Professions Division, New York.

Körding, K.P., Wolpert, D.M., 2004. Bayesian integration in sensorimotor learning. Nature 427 (6971), 244–247.

Kuo, A.D., 2005. An optimal state estimation model of sensory integration in human postural balance. Journal of Neural Engineering 2 (3), S235–S249.

Liang, J., Westheimer, G., 1993. Method for measuring visual resolution at the retinal level. Journal of the Optical Society of America A—Optics Image Science and Vision 10 (8), 1691–1696.

Macefield, V.G., Johansson, R.S., 1996. Control of grip force during restraint of an object held between finger and thumb: responses of muscle and joint afferents from the digits. Experimental Brain Research 108 (1), 172–184.

Paillard, J., 1996. Fast and slow feedback loops for the visual correction of spatial errors in a pointing task: a reappraisal. Canadian Journal of Physiology and Pharmacology 74 (4), 401–417.

Prablanc, C., Martin, O., 1992. Automatic-control during hand reaching at undetected 2-dimensional target displacements. Journal of Neurophysiology 67 (2), 455–469.

Saunders, J.A., Knill, D.C., 2004. Visual feedback control of hand movements. Journal of Neuroscience 24 (13), 3223–3234.

Sober, S.J., Sabes, P.N., 2005. Flexible strategies for sensory integration during motor planning. Nature Neuroscience 8 (4), 490–497.

Stein, G., 2003. Respect the unstable. IEEE Control Systems Magazine 23 (4), 12–25.

Timoshenko, S., 1961. Theory of Elastic Stability. McGraw-Hill, New York.

Todorov, E., 2004. Optimality principles in sensorimotor control. Nature Neuroscience 7 (9), 907–915.

Valero-Cuevas, F.J., 2000. Device for developing and measuring grasping force and grasping dexterity. United States Patent.

Valero-Cuevas, F.J., 2005. An integrative approach to the biomechanical function and neuromuscular control of the fingers. Journal of Biomechanics 38 (4), 673–684.

Valero-Cuevas, F.J., Smaby, N., Venkadesan, M., Peterson, M., Wright, T., 2003. The strength-dexterity test as a measure of dynamic pinch performance. Journal of Biomechanics 36 (2), 265–270.

Valero-Cuevas, F.J., Galván, A., Oliveira, M.E.d., Venkadesan, M., Laboissiére, R., 2006. Estimation of neurally modulated finger mechanical properties during dynamic manipulation via discrete perturbations. In: 36th Annual Meeting of the Society for Neuroscience. Atlanta, GA, 451.15/X22.

van Beers, R.J., Baraduc, P., Wolpert, D.M., 2002. Role of uncertainty in sensorimotor control. Philosophical Transactions of the Royal Society of London Series B—Biological Sciences 357 (1424), 1137–1145.

van der Kooij, H., Jacobs, R., Koopman, B., Grootenboer, H., 1999. A multisensory integration model of human stance control. Biological Cybernetics 80 (5), 299–308.

Venkadesan, M., Backus, S., Mandl, L.A., Swigart, A., Peterson, M., Lyman, S., Ariola, L., Hotchkiss, R.N., Valero-Cuevas, F.J., 2005. The strength-dexterity test is a novel and clinically informative measure of treatment outcome in thumb osteoarthritis. Arthritis and Rheumatism 52 (9), S516.

Wheat, H.E., Goodwin, A.W., Browning, A.S., 1995. Tactile resolution: peripheral neural mechanisms underlying the human capacity to determine positions of objects contacting the fingerpad. Journal of Neuroscience 15 (8), 5582–5595.

Wolpert, D.M., Ghahramani, Z., Jordan, M.I., 1995. An internal model for sensorimotor integration. Science 269 (5232), 1880–1882.

Supplementary Notes

Manipulating the edge of instability

Madhusudhan Venkadesan   John Guckenheimer
Francisco J. Valero-Cuevas

In this supplementary note, we provide details of the numerical optimization used for finding task-optimal sensory weights. To achieve this, we first mathematically define stability (i.e., the constraints) and the objective function (i.e., the goal) for our model. We then provide an alternate graphical representation of the optimization problem and its results using a 2D 'fitness landscape'.

1   Metrics for stability: "Survival times" and "Success rates"

We first define stability for the noisy, time-delayed model so that it agrees with the experimental notion of stability, namely, a compression was successful so long as it did not slip for a finite period of time. Stability in linear and nonlinear deterministic dynamical systems is a well-defined notion, either in the sense of asymptotic or Lyapunov stability (Doyle et al., 1992; Ogata, 2002; Guckenheimer and Holmes, 1983). For example, defining stability in the local sense (near a specific state of the system) is easily done for a hyperbolic fixed point[1] if the system under consideration is described either by ordinary differential equations (Doyle et al., 1992; Ogata, 2002;

---

[1]The term hyperbolic refers to the requirement that none of the eigenvalues of the linearization near the fixed point of interest lie on the imaginary axis. In other words, the system can be stable or unstable in different directions, but not marginally stable in any direction.

1

Guckenheimer and Holmes, 1983) or by delayed differential equations (i.e., systems with time-delay) (Kolmanovskii and Nosov, 1986; Kolmanovskii and Myshkis, 1999; Engelborghs et al., 2000, 2002). However, when there is some source of noise in the dynamic system, stability is often defined in terms of stationary distributions, i.e., using steady-state distributions of time spent in various parts of the phase space of the dynamical system. For some dynamical systems that are modeled using stochastic differential equations, the stationary distribution can be analytically derived using the Fokker-Planck equations (Soize, 1994). However, for most complex dynamical systems, the true distributions are approximated using statistical histograms that are obtained through large ensemble simulations of the given stochastic dynamic system. For example, one could define stability for a noisy system based on distributions of the time spent by trajectories of a stochastic system in different parts of its phase space (Arnold, 1998). Numerically, this could be calculated by simulating large ensembles of the noisy dynamic system and thus obtaining histograms of time spent in different regions (if these distributions converge to stationary distributions). Peaks in the distribution (i.e., "representative" locations) can then be called as "stable" points in the phase space of the dynamical system.

However, in the context of our system, there is an alternate "natural" definition of stability that arises from the task requirement for subjects in the experiments. We called the experimental behavior as "stable" or "successful" if the subjects could prevent the spring from slipping for a finite time period (7s). This definition of "success" in our task naturally lends itself to "be studied in the context of a survival, or first passage, time problem" (Cabrera and Milton, 2004), terms that we define below.

1.1   Definitions of success rate and survival time

The first observation is that if a trajectory (time-series of θ – rotation angle of the spring's endcap; Figure 1, left) leaves the domain of attraction (region enclosed by dashed red curves in Figure 1 on Page 4) and never returns inside it during the 7s period (let us name it T^*), then it almost certainly reached one or the other undesirable stable fixed points (at $\theta \approx$ 0.5rad; solid red curves in Figure 1) and thus, the spring "slipped". So, we can define 'success-rate' (p_{success}) as the probability that the time (t_{exit}) at which the θ trajectory exits the domain of attraction (to never return again)

2

is greater than T^* (the desired duration of the hold phase, namely 7s).

$$t_{\text{exit}} = \min\{T; \text{such that } \theta(t > T) \notin [\theta_0 - \delta\theta, \theta_0 + \delta\theta]\} \qquad (1)$$
$$p_{\text{success}} = p(t_{\text{exit}} \geq T^*) \qquad (2)$$

where, $\delta\theta$ defines the domain of attraction and p_{success} is the 'success-rate'. The time t_{exit} is called the 'survival time'. Based on approximate estimates (not shown) from experimental data that after training subjects slipped in approximately 20% of the trials, we chose a nominal value of $p^* = 0.8$ for the success-rate to define a "successful compression" in our model. The utilization of p^* in our model will become clear when we define F_s below. For experimental trials, F_s is the maximal sustained load for 7s. Nevertheless, it is important to note that in our simulations we calculate p_{success} by using large ensembles of simulations and calculating the fraction of the ensemble that are 'stable' (p_{success}) in the sense that $t_{\text{exit}} \geq T^*$.

1.2 Definition of F_s in the model

For given sensory weights, the success rate (p_{success}) depends on the value of F_s. Symbolically, $p_{\text{success}} = p_{\text{success}}(F_s)|_{(\omega_1, \omega_2, \omega_3)}$, i.e., for given sensory weights, p_{success} is a well-defined function of F_s. Hence, we can define F_s for a successful compression in our model as the solution to the 'root finding' problem,

$$p_{\text{success}}(F_s)|_{(\omega_1, \omega_2, \omega_3)} = p^* \qquad (3)$$

Numerically, we implemented this root finding problem using an adapted version of the Newton-Raphson method. Note that by defining F_s in this manner, it is implicitly (through the definition of p_{success}) an expected value, i.e., a metric of average performance and not single-trial performance. We have thus explained how F_s is defined. We will explain how to calculate sensory weights (i.e., $(\omega_1, \omega_2, \omega_3)$) that maximize F_s in Section 2 below.

1.3 Numerical integration of stochastic delay differential equations

Numerical integration of the one-dimensional stochastic delay differential equation (SDDE) was carried out using a simple Euler integration scheme (Küchler and Platen, 2000). As shown by Küchler and Platen (2000), for the
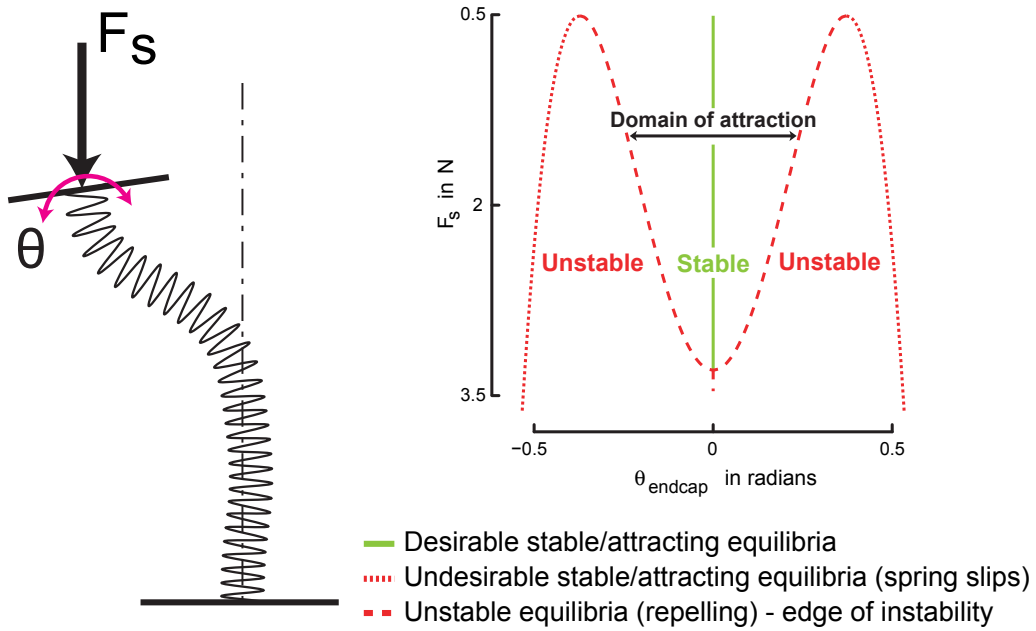
Figure 1: The loci of stable (solid green line) and unstable / undesirable (red dashed / dotted curves) equilibria for the thumb + spring + nervous system's closed loop dynamics without noise or time-delays as the spring is compressed. This figure is a succinct description of the underlying deterministic (no time-delays / noise) dynamics of the subcritical pitchfork bifurcation's normal form equation.

case of additive noise, the Euler integration scheme has a strong order of convergence 1.0. The term 'strong order' just refers to the fact that if the 'true' solution to the SDDE was known for a specific instance of the noisy processes in the system, then, with smaller and smaller time-steps, the numerically integrated solution converges to the true solution. This is different from weakly convergent numerical techniques, where the average of some function of the solution converges to the 'true' value, but each individual solution might itself not converge. We will not say more about numerical techniques for integrating SDDEs since the paper by Küchler and Platen (2000) and the references cited by them provide a good reference for numerical integration of SDDEs.

2 Numerical optimization: sensory weights that maximize F_s

We now outline the numerical optimization procedure used to compute task-optimal sensory weights. There are only three sensory weights that need to be found by our optimization routine that maximizes F_s. Given the additional constraint that the sum of the sensory weights is one, the optimization problem reduces to a 2-parameter optimization problem, namely,

$$\max_{\omega_1, \omega_2, \omega_3} F_s \text{ such that } \sum_{i=1}^{3} \omega_i = 1 \text{ and } p_{\text{success}}(F_s)|_{\omega_1, \omega_2, \omega_3} = 0.8 \qquad (4)$$

This is amenable to a global parameter search. We discretized the plane defined by $\omega_1 + \omega_2 + \omega_3 = 1$ in the positive octant of the space of sensory weights using a fine grid and numerically calculated F_s at each grid point. Thus, we found task-optimal performance and sensory weights for every sensory occlusion condition.

3 Sensory weights that minimize the effects of noise alone

To quantify the impact of time-delays on sensory weighting, we performed simulations using noise-minimizing sensory weights in addition to task-optimal sensory weights (that emerge from the combined effect of noise

and time-delays. Any deficit in performance (F_s) and deviation from exper-
imental measurements that arise from using sensory weights that minimize
the effects of noise alone can then be attributed to time-delays. The sensory
weights that minimize the effect of noise alone are obtained using Bayesian
inference for static tasks, i.e.,

$$\omega_i = \frac{1/\sigma_i^2}{\sum_j \left(1/\sigma_j^2\right)} \tag{5}$$

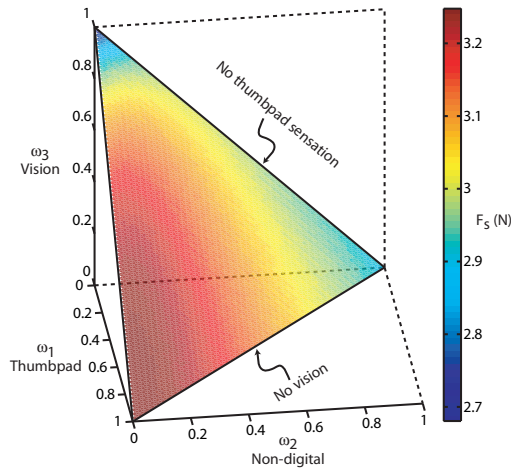where, σ_i^2 are the variances associated with each sensory channel.

Figure 2: Results of the global optimization using the *65ms simulation*. The
edges corresponding to the no vision and no thumbpad sensation conditions
are marked in the figure. Note how tactile sensation dominates the landscape
when it is available (dark red region). Keep in mind that the vertices of the
triangular planar surface of feasible sensory weights are the case when one
sensory channel is used exclusively.

4   Fitness landscape representation of simula-
tion results

The results of the global optimization are shown as contour plots for
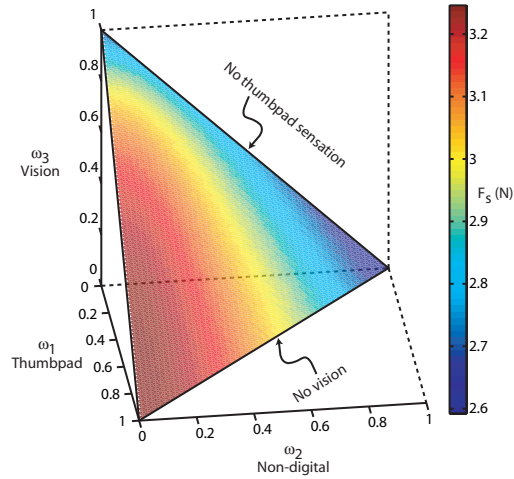both the *65ms simulation* (Figure 2) and the *100ms simulation* (Figure 3)

Figure 3: Results of the global optimization using the *100ms simulation*. Note how the peak in F_s for the no thumbpad sensation condition shifts slightly closer to the "vision corner" for the *100ms simulation* compared to the *65ms simulation* (Figure 2).

as an alternate representation of the results presented in the main text to clarify how the task-optimal sensory weights were found. The triangular planar surface in the contour plots are the set of feasible sensory weights, i.e., sensory weights that satisfy both the constraints $\omega_1 + \omega_2 + \omega_3 = 1$ and $\omega_i > 0$ for $i = 1, 2, 3$. The color coding depicts F_s according to the definition given in Equation (3) on Page 3 at each point on the plane.

References

L. Arnold. *Random dynamical systems*. Springer monographs in mathematics. Springer, Berlin ; New York, 1998.

J. L. Cabrera and J. Milton. Stick balancing: On-off intermittency and survival times. *Nonlinear Studies*, 11(3):305–317, 2004.

J. C. Doyle, B. A. Francis, and A. Tannenbaum. *Feedback control theory*. Toronto, New York Macmillan Pub. Co., 1992.

K. Engelborghs, T. Luzyanina, and D. Roose. Numerical bifurcation analy-

sis of delay differential equations. *Journal of Computational and Applied Mathematics*, 125(1-2):265–275, 2000.

K. Engelborghs, T. Luzyanina, and D. Roose. Numerical bifurcation analysis of delay differential equations using dde-biftool. *ACM Transactions on Mathematical Software*, 28(1):1–21, 2002.

J. Guckenheimer and P. Holmes. *Nonlinear oscillations, dynamical systems, and bifurcations of vector fields*. Springer, New York, corr. 7th print. edition, 1983.

V. B. Kolmanovskii and A. D. Myshkis. *Introduction to the theory and applications of functional differential equations*. Mathematics and its applications ;; v. 463; Variation: Mathematics and its applications (Kluwer Academic Publishers) ;; v. 463. Boston, Dordrecht, 1999.

V. B. Kolmanovskii and V. R. Nosov. *Stability of functional differential equations*. Mathematics in science and engineering ;; v. 180;. Orlando, London, 1986.

U. Küchler and E. Platen. Strong discrete time approximation of stochastic differential equations with time delay. *Mathematics and Computers in Simulation*, 54(1-3):189–205, 2000.

K. Ogata. *Modern control engineering*. Prentice Hall, Upper Saddle River, NJ, 4th edition, 2002.

C. Soize. *The Fokker-Planck equation for stochastic dynamical systems and its explicit steady state solutions*. Series on advances in mathematics for applied sciences ;; v. 17;. Teaneck, N.J., Singapore, 1994.